

Year 3 - CY2020 Allocation Renewal

1 Project Achievements in Years 1 and 2

1.1 Significant Accomplishments and Progress on Project Milestones

1.1.1 3D simulations of magnetorotational core-collapse supernovae

One of the key objectives for Year 1 of our INCITE project was to execute a parameter study of magnetorotational core-collapse supernova (CCSN) simulations using high-fidelity neutrino transport and magnetohydrodynamics (MHD) as implemented in our Spark-M1 application, built in the FLASH simulation framework (Fryxell et al., 2000; Dubey et al., 2009). Spark-M1 utilizes the new Spark high-order MHD solver (Couch, 2017), the M1 two-moment explicit neutrino transport method (Shibata & Taniguchi, 2011; O'Connor, 2015; O'Connor & Couch, 2018b), an accurate and efficient multipole gravity solver (Couch, 2013) including the general relativistic monopole correction (Marek et al., 2006), and the FLASH framework for adaptive mesh refinement (AMR), I/O, and runtime management. The methods and physics included in Spark-M1 make it one of the most high-fidelity and high-performance CCSN simulation tools in the world.

The Spark MHD solver (Couch, 2019) implements the cell-centered method of generalized Lagrangian multipliers (GLM; Dedner et al., 2002; Mignone et al., 2010) to control the growth of the divergence of the magnetic field. The GLM-MHD scheme employs hyperbolic advection and parabolic damping of divergence errors in order to avoid expensive elliptic divergence cleaning (e.g., Jiang & Wu, 1999) or complicated staggered-mesh constrained transport (e.g., Gardiner & Stone, 2005; Lee et al., 2009; Lee, 2013). Spark implements the GLM-MHD scheme via a finite-volume approach using high-order primitive reconstruction, multiple Riemann solvers for flux calculation, and method-of-lines time integration using multi-stage strong stability preserving (SSP) low-storage Runge-Kutta (RK) integrators of second- and third-order (e.g., Gottlieb & Shu, 1998). For realistic, non-Gamma-law equations of state, Spark avoids the approach of Colella & Glaz (1985) used in other FLASH solvers and adopts the volumetric internal energy, ρe , as an auxiliary thermodynamic primitive variable instead, as in Almgren et al. (2010). We have found this approach to be generally more robust but either method should be technically equivalent (e.g., Zingale & Katz, 2015). For our CCSN application, we use fifth-order WENO reconstruction (Borges et al., 2008), second-order time integration, and the HLLC approximate Riemann solver

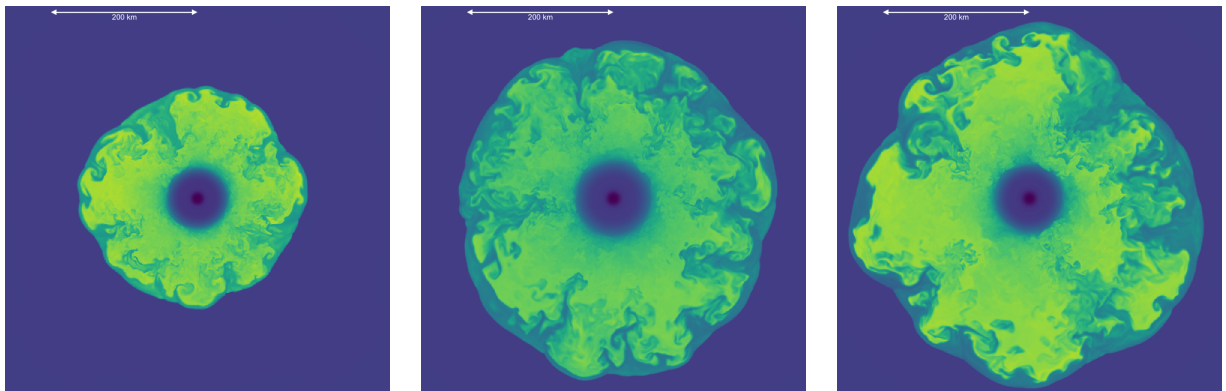


Figure 1: Slice plots of entropy from three of the 3D magnetorotational CCSN simulations that we ran on *Mira* as part of this INCITE project. Shown are cases with no magnetic fields or rotation (left), rotation but no magnetic fields (middle), and rotating and magnetic (right). In this plots, all simulations are currently at around 250 ms post-bounce.

(Toro, 2009).

Neutrino transport in Spark-M1 is carried out using the M1 two-moment explicit approach described in O’Connor (2015); O’Connor & Couch (2018b,a). The M1 scheme solves the first two angular moments of the Boltzmann equation for neutrinos and utilizes an analytic closure for the higher-order moments. The neutrino fluxes, both in real space and in energy space, are computed explicitly as a hyperbolic system resulting in favorable performance and scaling properties (at the cost of time step sizes limited by the speed of light) while the matter-radiation source terms are computed implicitly. This implicit solve is completely local and requires solving only a 4x4 matrix. Our M1 solver is fully velocity-dependent, except in the calculation of the explicit flux terms, which is done to $\mathcal{O}(v/c)$. In Year 1, we did not include inelastic neutrino scattering in the multi-dimensional version of our transport solver but during Year 2 we have successfully implemented and optimized this capability and will use it in the production simulations planned for Year 3.

The two-moment M1 approach is inherently more accurate than zeroth-moment only approaches such as flux-limited diffusion (e.g., Bruenn et al., 2013; Dolence et al., 2015; Lentz et al., 2015). M1 does not require a flux-limiter-based closure for the radiation fluxes as they are solved for directly. Furthermore, the analytic closure we currently use for the moments beyond the first is simple and straightforward yet shows encouraging agreement with 1D Boltzmann and Monte Carlo neutrino transport calculations (O’Connor, 2015; Murchikova et al., 2017). As compared with flux-limited diffusion, M1 does not suffer from the inability to capture “shadows” inherent to FLD schemes. A known limitation of M1 is cases in which distinct beams of radiation intersect, causing radiation “shocks.” The M1 solution in such cases becomes highly diffuse at the intersection. This is a problem in, e.g., radiation hydrodynamic calculations of accretion disks or neutron star mergers. For CCSNe, however, the radiation field is highly forward peaked and cases in which distinct beams of radiation might cross are essentially non-existent. Hence, M1 is *ideally* suited for the CCSN problem due to its accuracy (for the specific problem) and efficiency. In addition, the severe limitation of time steps determined by the speed of light is not so drastic in CCSNe since the explicit time step is already just a factor of a few larger than this thanks to the enormous sound speeds in the proto-neutron star (PNS). Another significant advantage of M1 is that it is a fully multidimensional transport scheme, i.e., the solution at a given grid point is dependent on the fluxes from every direction around that point. This is distinct from the often-adopted “ray-by-ray” approximation (e.g., Bruenn et al., 2013, 2016; Müller et al., 2012; Hanke et al., 2013; Melson et al., 2015; Lentz et al., 2015) in which the transport problem is solved only along discrete radial rays. The advantages of M1 for neutrino transport in CCSNe have not gone unnoticed and a number of groups are now adopting this approach (Just et al., 2015; Kuroda et al., 2016; Skinner et al., 2016; Roberts et al., 2016; Vartanyan et al., 2018, 2019).

In our FLASH CCSN application we have assumed that the composition of the matter throughout the entire computational domain is determined by nuclear statistical equilibrium (NSE). This common approximation (e.g., Burrows et al., 2007; Ott et al., 2008; Dolence et al., 2015; Skinner et al., 2016; Roberts et al., 2016; Kuroda et al., 2016) is appropriate at high densities and temperatures where the nuclear reaction rates are sufficiently fast to establish equilibrium essentially instantly but becomes increasingly incorrect at low densities such as those in the silicon and oxygen shells surrounding the collapsing iron core. Critically, correctly predicting the explosion energy or nucleosynthetic products such as radioactive nickel can be severely impacted by the inappropriate assumption of NSE (Bruenn et al., 2016). Bruenn et al. (2016) advocate the use of an approximate nuclear network in regions that are not in NSE, while other groups (e.g., Müller et al.,

2012; Melson et al., 2015) use a “flashing” approach rather than a full network calculation. We have recently implemented a method for transitioning to a nuclear network and appropriate EOS at low densities. Our new approach blends the pressures between the high- and low-density EOS’s to prevent spurious pressure discontinuities and uses an auxiliary variable to track whether a zone is entering or exiting NSE, allowing us to appropriately set the composition in the transition region. This new capability will be included in Year 3 production simulations.

In Year 1, we successfully executed a parameter study of magnetorotational CCSN simulations. Figure 1 shows volume renderings of entropy from three of the five high-resolution 3D simulations we ran on *Mira* and *Theta*. We opted to use the $15-M_{\odot}$ progenitor from Heger et al. (2005) in order to facilitate a direct comparison to the recent results of Summa et al. (2018). We ran five different cases for this one progenitor: (1) non-rotating, non-magnetic; (2) rotating, non-magnetic; (3) non-rotating, magnetic; (4) rotating, magnetic; and (5) rapidly rotating, non-magnetic. For rotating cases, we take the rotation profile directly from the progenitor model that was evolved with rotation and magnetic fields and prescriptions for angular momentum transport (Heger et al., 2005). For the rapidly-rotating case, we simply multiply the angular speed of the profile by two, making the rate of rotation similar to one of the models explored by Summa et al. (2018). The magnetic field is initialized with a quasi-poloidal field geometry with the peak strength set to match the field strength of the original progenitor model, about 10^8 G. The peak angular speed of this model is about 0.2 rad s^{-1} (0.4 rad s^{-1} for the “rapidly” rotating case). This is, in fact, not very rapid rotation or field strength and so in these models we do not expect to see dramatic, magnetorotationally-dominated dynamics. Rather, we explored the impact of plausibly typical rotation rates and field strengths on the CCSN mechanism.

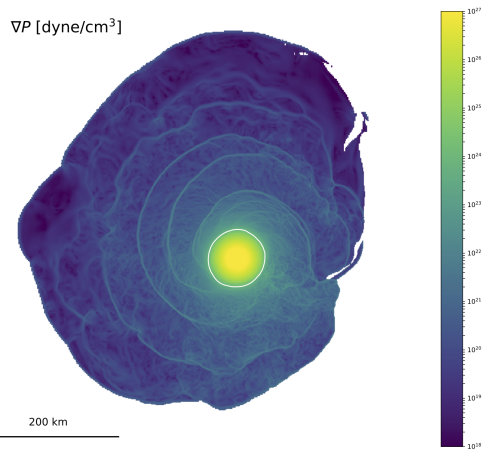


Figure 2: Equatorial slice plot of the gradient of pressure from a 3D magnetorotational CCSN simulation run as part of our previous INCITE project. The development of a non-axisymmetric rotational instability in the PNS leads to the generation of strong spiral pressure waves. The gravitational wave emission is also significantly amplified.

Detailed analysis and comparisons are underway

Our results from Year 1 simulations indicate that the presence of rotation, in particular, is helpful to CCSN shock revival (e.g., Summa et al., 2018). As shown in 1, the addition of rotation substantially increases the mean shock radius at the same time post-bounce. For the non-rotating, non-magnetic case (left panel), the shock is already receding by this point whereas for all cases including rotation the shock remains stalled at large radii (~ 200 km). The right panel of Figure 1 shows the case including both realistic rotation and weak initial magnetic fields. The magnetic fields, even if weak, may still have an impact on the behavior of the turbulence in the gain region and the PNS. Indeed, we see that while the field strengths, even at this point post-bounce, are not dynamically strong, there is still a noticeable impact on the overall evolution of the simulation. The shock is at slightly larger radii than the rotating-only case and the entropies in the gain layer are on average greater. This simulation is closer to explosion than the comparable case without magnetic fields. De-

ence of a non-axisymmetric rotational instability in the PNS (Wheeler & Akiyama, 2007; Ott et al., 2005). In work based on simulations ran as part of our previous INCITE allocation, we have identified the emergence of such an instability for magnetic and rotating initial conditions. This instability can generate strong pressure waves that transport energy to the gain region, and also leads to very loud gravitational wave signals. An image of the strong pressure waves is shown in Figure 2.

1.1.2 3D Simulations of CCSN Progenitors

One of the most remarkable and exciting results of recent 3D simulations of the CCSN mechanism is the discovery that realistic non-spherical structure in the progenitor star can have a dramatic impact (Couch & Ott, 2013; Couch et al., 2015; Couch & Ott, 2015; Müller & Janka, 2015; Müller et al., 2017; O’Connor & Couch, 2018a). The breaking of spherical symmetry is manifest in the turbulent convection driven by nuclear burning in the cores of massive stars. As a massive star nears collapse, strongly convective burning in the Si and O shells surrounding the iron core can reach speeds of nearly 1000 km s^{-1} and is characteristically very large in spatial scale (Arnett & Meakin, 2011; Couch & Ott, 2015; Müller et al., 2016). These convective perturbations will reach the stalled shock shortly after core bounce and can aid neutrino-driven explosions by either enhancing the strength of post-shock turbulence (Couch et al., 2015) or causing large scale “forced shock deformations” (Müller et al., 2017), or both. These results serve to remind us that CCSN mechanism simulations are initial value problems and that the details of our initial conditions matter tremendously! Our work inaugurated the era of detailed investigation into the impact of 3D progenitor structure on the CCSN mechanism (Couch & Ott, 2013, 2015). As part of this INCITE project we are advancing the investigation into 3D progenitor structure substantially. Specifically, we are simulating 3D progenitors including rotation and magnetic fields.

A key milestone for Years 1 and 2 was to carry out new, high-fidelity 3D simulations of the final minutes of stellar evolution to the point of iron core collapse. We are used 1D massive star evolution models constructed using MESA (Paxton et al., 2011, 2013, 2015), initialized in 3D approximately five minutes prior to core collapse. During Years 1 and 2 we ran a full-3D non-rotating, non-magnetic case all the way to the point of iron core collapse. In second half of Year 2 we will carry out a second full 3D model that includes both rotation and magnetic fields. Our test simulations executed showed that the expense of the simulations increases significantly as the stars approach collapse. This is due to more vigorous nuclear burning in the core, increasing the expense of the nuclear network solve. Therefore, in order to ensure that we can simulate sufficiently long time scales, we have opted to execute just these two simulations rather than the originally-planned four.

In Years 1 and 2, we made substantial gains in

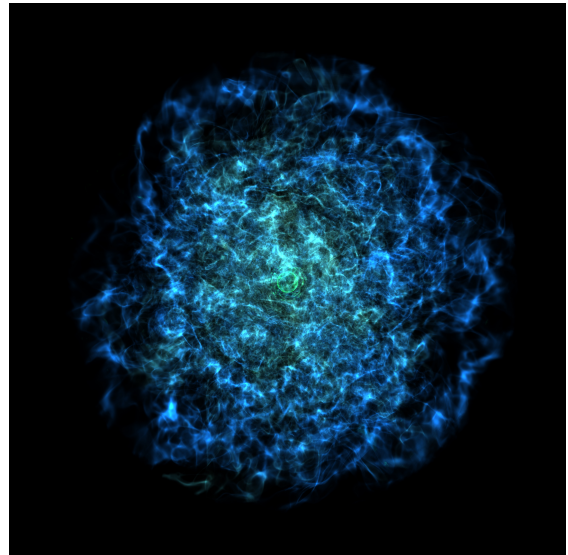


Figure 3: Volume rendering of the velocity magnitude from a 3D progenitor simulation run in full “ 4π ” geometry during Years 1 and 2 of this project. Peak convective speeds reach over 300 km/s prior to core collapse. This simulation is being used as initial conditions for Year 2 CCSN simulations.

improving our simulation approach for 3D CCSN progenitors. We improved the OpenMP threading of our nuclear network code. We improved the efficiency of the empirical load balancing approach our progenitor application uses. We tested several approaches to the initial mapping of the 1D progenitor model to the 3D domain and have improved our approach to stabilizes the initial conditions. We implemented new, modern reaction rates for electron captures and for key carbon reactions. And, importantly, we have successfully, and efficiently, run a full production simulation all the way to core instability and collapse.

For the rotating, magnetic progenitor we are using a MESA model constructed using the magnetic field production and angular momentum transport model of [Spruit \(2002\)](#), as implemented for stellar evolution by [Heger et al. \(2005\)](#); [Paxton et al. \(2015\)](#). This model yields a realistic rotation profile and an estimate for the *strength* of the magnetic field as a function of radius in the star. There is very limited information about the 3D geometry of the field. To address this, we are initializing the field in a random, divergenceless fashion with a typical strength matching the 1D MESA model estimate. We will then allow the field to relax to a quasi-steady-state configuration. This transition should occur on the rotational and convective time scale, both of which are about 30 s. We will simulate roughly 3 to 5 minutes of evolution up to core collapse.

1.1.3 High-resolution Simulation of Magnetorotational Turbulence

Our final simulation milestone for Year 1 was to execute a high-resolution simulation of magnetorotational turbulence in the CCSN gain region. For this simulation, we used the “rapidly” rotating conditions described above and allow for higher resolution in the gain layer using AMR. This simulation required many more zones than the fiducial resolution case and was a standalone Capability-scale simulation. This simulation was run until 100 ms post-bounce and we are now analyzing the results and comparing to the lower-resolution case.

1.1.4 Long time simulations of MHD CCSNe

In Year 2 of this project we are carrying out the 3D simulations of magnetorotational CCSNe from Year 1 to late times, nearing one second post-bounce. Long time scale simulations are crucial for accurately predicting the explosion energy, PNS mass, nucleosynthesis, etc. ([Bruenn et al., 2016](#); [Müller et al., 2017](#)). For any of the simulations that fail to explode, we will attempt to simulate late enough times to capture the onset of PNS collapse to a black hole. This has the potential to elucidate some details of the formation of stellar mass black holes, such as those that have been detected by aLIGO ([Abbott et al., 2016, 2017](#)). We have recently shown ([Pan et al., 2018](#)) that the GR effective potential approach can fairly accurately predict black hole formation time in 2D as compared to 1D fully GR simulations ([O’Connor & Ott, 2011](#)).

The nucleosynthetic yields from CCSN simulations are a key quantity that can be directly compared to observations and laboratory measurements of cosmic abundances. We will compute the detailed nucleosynthesis from these late-time CCSN simulations. This will be accomplished as a post-processing step using the open-source SkyNet nuclear reaction network code developed by Co-I Roberts. The input for the nuclear reaction networks will be passive tracer particle data that records thermodynamic trajectory information from our FLASH CCSN simulations. FLASH already includes a well-developed, efficient passive-particle framework that has been used extensively in the calculation of nucleosynthesis in Type Ia supernova simulations (e.g., [Long et al., 2014](#)). We will compute detailed abundances for elements such as radioactive nickel and titanium, two key observable quantities, and we will also examine how rotation and magnetic fields can

influence the conditions for very heavy element formation and the r-process.

These simulations have been restarted from simulations carried over from Year 1 and are running in the Capability queue on *Mira*. Substantial progress has been made on these simulations and they are nearing completion.

1.1.5 High-resolution simulation of MHD dynamos in the proto-neutron star

There is a very strong shear layer at the edge of rotating PNS's that is unstable to the magnetorotational instability (MRI, [Akiyama et al., 2003](#); [Burrows et al., 2007](#)). The presence of convection combined with rotation in the PNS can also lead to an $\alpha\text{-}\Omega$ dynamo ([Mösta et al., 2015](#)). Both mechanisms can lead to exponential amplification of magnetic fields with dramatic implications for the CCSN mechanism. Accurately capturing either process is extremely challenging computationally, requiring extremely high resolution to capture the fastest growing modes of these instabilities ([Mösta et al., 2015](#)). In Year 2 of this project, we will carry out an extremely high resolution simulation of a rotating PNS in order to study the rapid growth of magnetic fields via the MRI and dynamo. This simulation will go beyond [Mösta et al. \(2015\)](#) in a number of ways: we will use our M1 neutrino transport method rather than leakage, we will include the entire solid angle of the sphere rather than just a 90° wedge, and will simulate to later times in the aim of capturing the saturation of the magnetic fields. Using AMR, we will add two extra levels of refinement beyond our fiducial resolution only in the shear layer surrounding the PNS, between 15 km and 40 km, bringing the finest resolution elements to 163 m. This approach was piloted for capturing turbulence in the gain region during our current INCITE project and will avoid adding additional zones in regions that are stable to the instabilities of interest. This is not as high as the highest resolution used by [Mösta et al. \(2015\)](#) but we plan to go to much longer time scales, as much as 100 ms post-bounce. This simulation will comprise about 100 million zones in 3D and require about 200,000 time steps to reach 100 ms.

So far in Year 2 we have analyzed simulations from Year 1 that will serve as the initial conditions for this high-resolution simulation. We anticipate starting this simulation in Q3 of Year 2. Given the extreme resolution of this simulation, it will run in the Capability queue from the outset.

1.1.6 MHD simulation of CCSN progenitors

In Year 2, we are extending the Year 1 study of iron core collapse to rotating and magnetic stars. We will simulate the final five minutes of stellar evolution to core collapse in 3D for a $25-M_{\odot}$ progenitor stars for both “high” and “low” core rotation rates. As in Year 1, all final models will be made publicly available.

These simulations will be started in Q3 of Year 2. We are now tuning our progenitor application to make better use of OpenMP threading and developing realistic initial conditions for the magnetic field strength and geometry.

1.1.7 CCSN simulation with 3D progenitors

In Year 2 we will use the 3D progenitor models generated in Year 1 for 3D CCSN simulations on *Theta*. The progenitor model for these simulations is now finished and ready to be used in CCSN simulations. For these simulations, we will enhance the physical fidelity of our neutrino transport by incorporating our newly-implemented neutrino-electron scattering capability and the latest, most accurate electron capture rates.

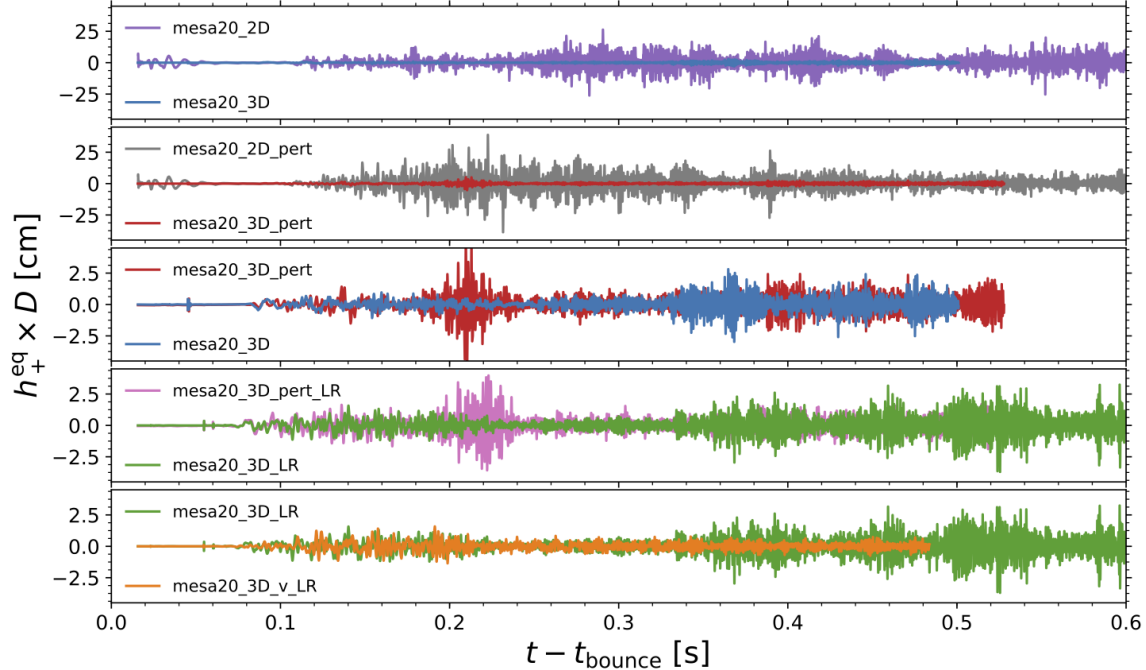


Figure 4: Gravitational wave strains from the 3D simulations of O’Connor & Couch (2018b), carried out under a prior INCITE award. Our work showed for the first time that the presence of 3D structure in the progenitor star leaves a detectable imprint on the gravitational wave emission.

1.1.8 Fundamentally 3D Phenomena in CCSNe

Recently, we submitted a publication detailing results based on simulations carried out under our previous INCITE award (O’Connor & Couch, 2018a). This work includes several full 3D, high-resolution simulations using our M1 neutrino transport in FLASH, representing over 100 Million core-hours of work on *Mira*. In these simulations, we identify and analyze several essentially 3D aspects of CCSNe, including the presence of a new instability in the neutrino emission called the Lepton-number Emission Self-sustaining Asymmetry (LESA), first reported by (Tamborra et al., 2014). We are the first group to confirm the presence of the LESA in CCSNe and, since we use a very different transport approach, our work strongly implies this is not a numerical artifact but a real physical instability.

In O’Connor & Couch (2018b), we also show that the presence of the non-spherical, 3D progenitor structure has several important impacts on the CCSN mechanism. We show that convective motion in the progenitor can substantially increase the proximity to explosion. We also showed that 3D structure in the progenitor can leave a measurable imprint on the gravitational wave emission from CCSNe that could be detected by, e.g., LIGO. The gravitational wave strains from our simulations are shown in Figure 4.

1.2 Project Usage

In Year 1 of our allocation, we fully expended our allocations on both *Mira* and *Theta* (see Figure 5). On *Theta*, despite a late start to our production simulations, we exceeded our initial allocation by 12%.

So far in 2019 we expended 66M core-hours on *Mira* out of our total 2019 allocation of 150M

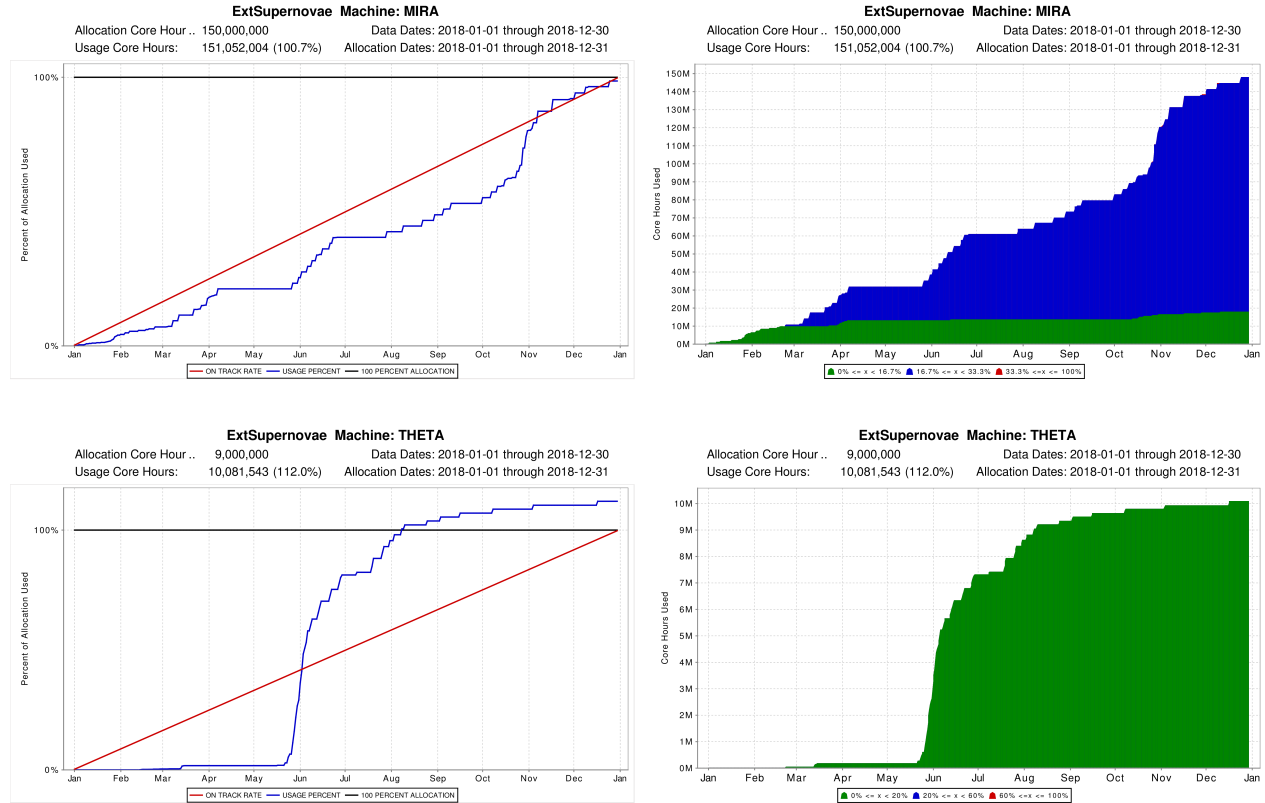


Figure 5: Allocation usage in Year 1 on *Mira* and *Theta*.

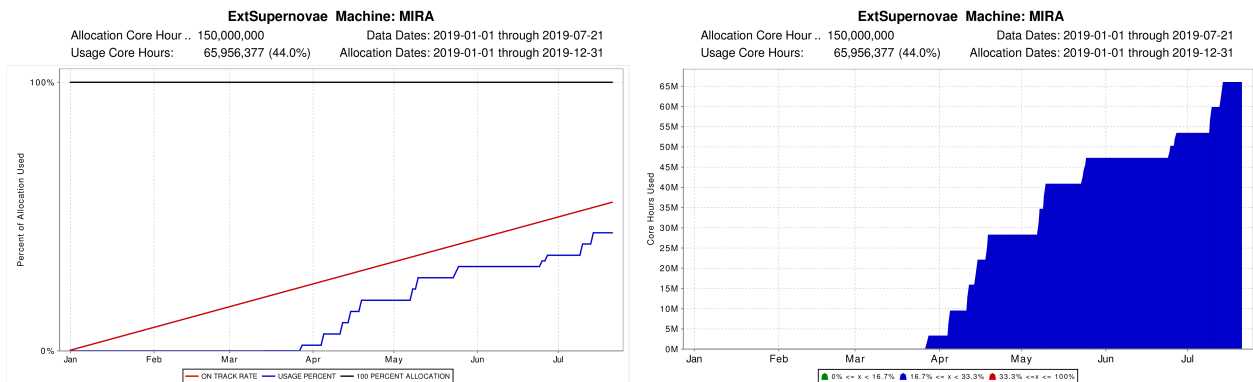


Figure 6: Allocation usage in Year 2 on *Mira*.

core-hours (44% usage). This is just slightly behind the linear usage curve, though our burn rate in Q2 was substantially larger than for Q1. We are now running one of our primary simulation milestones in the Capability queue and will start a second Capability-scale simulation in the next week or two. Figure 6 we show our current usage and categorized hours on Mira.

We have yet to start running production simulations on Theta for two reasons. First, during Q1 we spent some effort continuing to tune our production application for Theta. This is largely complete now. The second reason for the delayed start is that we were waiting on the completion of 3D supernovae progenitor simulations that we had planned to use as the initial conditions for our simulations on Theta this year. These simulations are now complete and a paper is in preparation describing them. We are now prepared to start these simulations during Q3. Based on our experience last year running on Theta, we do not anticipate any difficulty in expending our entire allocation before the end of the calendar year.

1.3 Application Parallel Performance

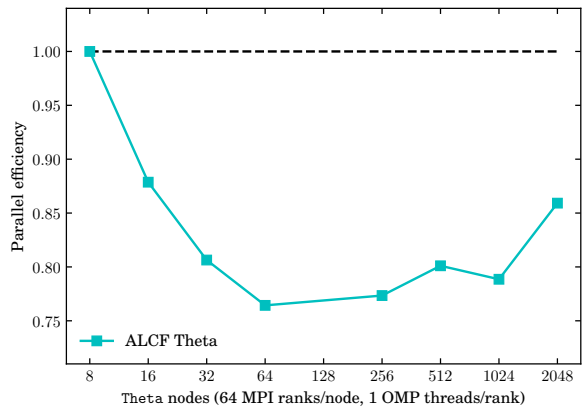


Figure 7: Weak scaling parallel efficiency of our Spark-M1 application on *Theta*.

As shown in our original proposal, our application demonstrates good parallel performance. In Figure 7 we show the weak scaling parallel efficiency of Spark-M1 on *Theta* for up to 2048 nodes. At production scales ($\gtrsim 128$ nodes), we see an efficiency of around 80%. Considering the immense communication requirements of our M1 transport solver, we consider this good performance.

We have also substantially improved our overall application performance on *Theta* during Years 1 and 2. At the time of our original proposal, Spark-M1 on *Theta* and a performance metric of 91 mega-zone-updates per node-hour. We have optimized the single-node performance of our application to better utilize KNL hardware threads,

high-bandwidth memory, and OpenMP parallelism. For the same application we now achieve a metric of 132 mega-zone-updates per node-hour, and increase in single-node performance of 44%.

We have also made significant progress on other code development relevant to, but not directly planned as part of, this INCITE program. In our neutrino transport, we have implemented neutrino-electron inelastic scattering, an important process that we have so far only included during the 1D collapse phase of our simulations. We have also begun porting our Spark MHD solver to the DOE Exascale Computing Project (ECP)-supported AMReX framework. We are doing this within the new version of FLASH that is being developed as part of the DOE ECP. We anticipate moving to the AMReX version of FLASH in the future for our production simulations.

The second major code development effort we performed in Year 2 is the implementation of high-order, single-step methods for MHD in our CCSN application. This is work also supported by the TEAMS SciDAC collaboration. Chelsea Harris, a new research associate at MSU, is leading this effort. Our Spark MHD solver is written in such a way to make implementation of this new approach straight-forward. A high-order single-step method will both increase the accuracy of our simulations while also decreasing the overall communication burden. This has the potential to significantly improve our computational efficiency. We will also continue porting our various

physics routines, particularly Spark, to the AMReX-capable version of FLASH.

1.4 Data Storage

At present, we have 280 TB of online storage on the *Mira* filesystem and approximately 200 TB on archival storage. At this stage, we are continually triaging our on-disk data and moving to tape as we are able to free up disk for new simulations.

2 Project Plans for Year 3

During Years 1 and 2 we have largely achieved our originally-planned goals for this three-year project. Therefore, our goals for Year 3 will be largely unchanged except for minor course corrections based on the actual achievements of the first two years. One major change is necessitated by the delay of the *Aurora* system. We had originally proposed an extensive parameter study of 3D magnetorotational CCSNe on *Aurora* for Year 3. We have opted to de-scope this study to far fewer simulations to be executed on *Theta* instead. This does require, however, a substantial increase in our request for *Theta* in Year 3. We had originally requested 500k node-hours on *Theta* in Year 3 but to achieve the goals we outline below we now request a total of 1M node-hours on *Theta* for 2020.

Based on our updated application performance studies on *Theta*, we estimate that for 500 ms of post-bounce evolution, our Spark-M1 CCSN simulations will require approximately 100k node-hours when including neutrino-electron scattering. This performance is very competitive with comparable state-of-the-art CCSN simulations on comparable hardware platforms ([Vartanyan et al., 2019](#)).

2.1 MHD CCSN Simulations Using 3D Progenitors

In Year 3 we will use the 3D progenitor models generated in Year 2 for 3D MHD CCSN simulations on *Theta*. These progenitors will be simulated in 3D with both rotation and magnetic fields. We will carry out two new CCSN simulations, one from a fully magnetorotational progenitor and one in a rotating-only progenitor. As with all planned Year 3 simulations, we include our newly-implemented neutrino-electron scattering capability. For this milestone we request a total of 250k node-hours and 40 TB of online storage.

2.2 Late time 3D Simulations of Magnetorotational CCSNe from 3D Progenitors

In Year 3 we will continue two CCSN simulations from 3D progenitors started in Year 2 to about one second post-bounce. As in Year 2, we will study the explosion energies, PNS masses, nucleosynthesis, and black hole formation times in these simulations as appropriate. For this milestone we request a total of 250k node-hours and 40 TB of online storage.

2.3 Magnetorotational CCSN Parameter Study in 3D Progenitors

The four 3D simulations planned above will be executed in progenitor models that have been evolved in 3D. At this point, those are the only such models we expect to be available, at least during the beginning of Year 3. In order to augment this progenitor set, and further explore the impact of rotation and magnetic fields across the range of potential CCSN progenitors, we will run four additional 3D CCSN simulations in the 1D magnetorotational progenitor models of ([Heger et al., 2005](#)). These models include realistic rotation profiles and rough estimates of magnetic field strengths. In order to increase the realism of these models in the absence of fully 3D evolution to core collapse, we will add multidimensional perturbations in the convective shells of these models

using the vector spherical harmonics formalism of Chatzopoulos et al. (2014). Such an approach has been used in several recent studies (O’Connor & Couch, 2018a; Vartanyan et al., 2019). We will select a range of progenitor compactnesses (O’Connor & Ott, 2011; Sukhbold et al., 2018) in this study. For these simulations, we will include inelastic neutrino scattering (O’Connor, 2015; Burrows et al., 2016). Each simulation will cost about 100k node-hours to reach around 500 ms post-bounce. Thus, we request a total of 500k node-hours and 80 TB of online storage for this milestone.

2.4 Code Development

For the planned Year 3 milestones above we require no further code development. The only major relevant development effort we plan to undertake in Year 3 is to continue to adapt our `Spark-M1` application to the new AMReX-based `FLASH5`. This version of `FLASH` is targeted at the exascale and is being supported by the DOE Exascale Computing Project.

References

- Abbott, B. P., Abbott, R., Abbott, T. D., et al. 2016, *Physical Review Letters*, 116, 061102
—. 2017, *Physical Review Letters*, 118, 221101
- Akiyama, S., Wheeler, J. C., Meier, D. L., & Lichtenstadt, I. 2003, *ApJ*, 584, 954
- Almgren, A. S., Beckner, V. E., Bell, J. B., et al. 2010, *ApJ*, 715, 1221
- Arnett, W. D., & Meakin, C. 2011, *ApJ*, 741, 33
- Borges, R., Carmona, M., Costa, B., & Don, W. S. 2008, *Journal of Computational Physics*, 227, 3191
- Bruenn, S. W., Mezzacappa, A., Hix, W. R., et al. 2013, *ApJ*, 767, L6
- Bruenn, S. W., Lentz, E. J., Hix, W. R., et al. 2016, *ApJ*, 818, 123
- Burrows, A., Dessart, L., Livne, E., Ott, C. D., & Murphy, J. 2007, *ApJ*, 664, 416
- Burrows, A., Vartanyan, D., Dolence, J. C., Skinner, M. A., & Radice, D. 2016, ArXiv e-prints
- Chatzopoulos, E., Graziani, C., & Couch, S. M. 2014, *ApJ*, 795, 92
- Colella, P., & Glaz, H. M. 1985, *Journal of Computational Physics*, 59, 264
- Couch, S. M. 2013, *ApJ*, 765, 29
—. 2017, *Philosophical Transactions of the Royal Society of London Series A*, 375, 20160271
—. 2019, in prep.
- Couch, S. M., Chatzopoulos, E., Arnett, W. D., & Timmes, F. X. 2015, *ApJ*, 808, L21
- Couch, S. M., & Ott, C. D. 2013, *ApJ*, 778, L7
—. 2015, *ApJ*, 799, 5
- Dedner, A., Kemm, F., Kröner, D., et al. 2002, *Journal of Computational Physics*, 175, 645
- Dolence, J. C., Burrows, A., & Zhang, W. 2015, *ApJ*, 800, 10
- Dubey, A., Antypas, K., Ganapathy, M. K., et al. 2009, *Parallel Computing*, 35, 512
- Fryxell, B., Olson, K., Ricker, P., et al. 2000, *ApJS*, 131, 273
- Gardiner, T. A., & Stone, J. M. 2005, *Journal of Computational Physics*, 205, 509
- Gottlieb, S., & Shu, C. W. 1998, *Mathematics of Computation*, 67, 73
- Hanke, F., Müller, B., Wongwathanarat, A., Marek, A., & Janka, H.-T. 2013, *ApJ*, 770, 66
- Heger, A., Woosley, S. E., & Spruit, H. C. 2005, *ApJ*, 626, 350

- Jiang, G.-S., & Wu, C.-c. 1999, Journal of Computational Physics, 150, 561
- Just, O., Obergaulinger, M., & Janka, H.-T. 2015, MNRAS, 453, 3386
- Kuroda, T., Takiwaki, T., & Kotake, K. 2016, ApJS, 222, 20
- Lee, D. 2013, Journal of Computational Physics, 243, 269
- Lee, W. H., Ramirez-Ruiz, E., & López-Cámara, D. 2009, ApJ, 699, L93
- Lentz, E. J., Bruenn, S. W., Hix, W. R., et al. 2015, ApJ, 807, L31
- Long, M., Jordan, IV, G. C., van Rossum, D. R., et al. 2014, ApJ, 789, 103
- Marek, A., Dimmelmeier, H., Janka, H.-T., Müller, E., & Buras, R. 2006, A&A, 445, 273
- Melson, T., Janka, H.-T., & Marek, A. 2015, ApJ, 801, L24
- Mignone, A., Tzeferacos, P., & Bodo, G. 2010, Journal of Computational Physics, 229, 5896
- Mösta, P., Ott, C. D., Radice, D., et al. 2015, Nature, 528, 376
- Müller, B., & Janka, H.-T. 2015, MNRAS, 448, 2141
- Müller, B., Melson, T., Heger, A., & Janka, H.-T. 2017, MNRAS, 472, 491
- Müller, B., Viallet, M., Heger, A., & Janka, H.-T. 2016, ApJ, 833, 124
- Müller, E., Janka, H.-T., & Wongwathanarat, A. 2012, A&A, 537, A63
- Murchikova, E. M., Abdikamalov, E., & Urbatsch, T. 2017, MNRAS, 469, 1725
- O'Connor, E. 2015, ApJS, 219, 24
- O'Connor, E., & Ott, C. D. 2011, ApJ, 730, 70
- O'Connor, E. P., & Couch, S. M. 2018a, ApJ, 865, 81
- . 2018b, ApJ, 854, 63
- Ott, C. D., Burrows, A., Dessart, L., & Livne, E. 2008, ApJ, 685, 1069
- Ott, C. D., Ou, S., Tohline, J. E., & Burrows, A. 2005, ApJ, 625, L119
- Pan, K.-C., Liebendörfer, M., Couch, S. M., & Thielemann, F.-K. 2018, ApJ, 857, 13
- Paxton, B., Bildsten, L., Dotter, A., et al. 2011, ApJS, 192, 3
- Paxton, B., Cantiello, M., Arras, P., et al. 2013, ApJS, 208, 4
- Paxton, B., Marchant, P., Schwab, J., et al. 2015, ApJS, 220, 15
- Roberts, L. F., Ott, C. D., Haas, R., et al. 2016, ApJ, 831, 98
- Shibata, M., & Taniguchi, K. 2011, Living Reviews in Relativity, 14, 6
- Skinner, M. A., Burrows, A., & Dolence, J. C. 2016, ApJ, 831, 81
- Spruit, H. C. 2002, A&A, 381, 923
- Sukhbold, T., Woosley, S. E., & Heger, A. 2018, ApJ, 860, 93
- Summa, A., Janka, H.-T., Melson, T., & Marek, A. 2018, ApJ, 852, 28
- Tamborra, I., Hanke, F., Janka, H.-T., et al. 2014, ApJ, 792, 96
- Toro, E. 2009, Riemann Solvers and Numerical Methods for Fluid Dynamics: A Practical Introduction (Springer Berlin Heidelberg)
- Vartanyan, D., Burrows, A., Radice, D., Skinner, M. A., & Dolence, J. 2018, MNRAS
- . 2019, MNRAS, 482, 351
- Wheeler, J. C., & Akiyama, S. 2007, ApJ, 654, 429
- Zingale, M., & Katz, M. P. 2015, ApJS, 216, 31